THE JOURNAL OF BIOLOGICAL CHEMISTRY Vol. 278, No. 30, Issue of July 25, pp. 27439–27448, 2003
Printed in U.S.A.

Kinetic Mechanism of Non-muscle Myosin IIB

FUNCTIONAL ADAPTATIONS FOR TENSION GENERATION AND MAINTENANCE*

Received for publication, March 11, 2003, and in revised form, April 14, 2003
Published, JBC Papers in Press, April 17, 2003, DOI 10.1074/jbc.M302510200

Fei Wang‡, Mihály Kovács‡, Aihua Hu, John Limouze, Estelle V. Harvey, and James R. Sellers§

From the Laboratory of Molecular Cardiology, NHLBI, National Institutes of Health, Bethesda, Maryland 20892-1762

Besides driving contraction of various types of muscle tissue, conventional (class II) myosins serve essential cellular functions and are ubiquitously expressed in eukaryotic cells. Three different isoforms in the human myosin complement have been identified as non-muscle class II myosins. Here we report the kinetic characterization of a human non-muscle myosin IIB subfragment-1 construct produced in the baculovirus expression system. Transient kinetic data show that most steps of the actomyosin ATPase cycle are slowed down compared with other class II myosins. The ADP affinity of subfragment-1 is unusually high even in the presence of actin filaments, and the rate of ADP release is close to the steady-state ATPase rate. Thus, non-muscle myosin IIB subfragment-1 spends a significantly higher proportion of its kinetic cycle strongly attached to actin than do the muscle myosins. This feature is even more pronounced at slightly elevated ADP levels, and it may be important in carrying out the cellular functions of this isoform working in small filamentous assemblies.

Myosins are a superfamily of actin-dependent molecular motors that can be subdivided into at least 18 classes based on sequence (1, 2). The "founding members" of this superfamily, the conventional filament-forming myosins that participate in muscle contraction and cytokinesis, are now classified as class II, including three whose products are typically found in the cytoskeleton and are not directly involved in muscle contraction. These three myosins are commonly called non-muscle myosins IIA, IIB, and IIC (NMIIA,[1] NMIIB, and NMIIC, respectively). Like their muscle myosin counterparts, these proteins are hexameric with two enzymatically active heads that interact with actin and ATP and a long tail formed by the dimerization of a coiled coil-forming sequence. Each of the two heads is associated with a pair of low molecular mass calmodulin-like light chains. NMIIC was recently found upon publication of the human genome, and little is known about its structure, function, or cellular localization (2). In contrast, the NMIIA and NMIIB proteins have been well studied (3–5). The expression of these isoforms is regulated in a cell- and tissue-specific manner (6, 7). For example, neuronal tissues are markedly enriched in NMIIB (8), whereas platelets contain only NMIIA (9). Immunofluorescent localization studies have shown that, in some cells, there is little overlap in the distribution of NMIIA and NMIIB, whereas in other cells, there is considerable overlap (9, 10). Both appear to be components of the contractile ring formed during cell division. Enzymatically, NMIIB is one of the slowest myosins in terms of its actin-activated MgATPase activity and the rate at which it translocates actin filaments *in vitro* (5, 11).

We show that NMIIB subfragment-1 (S1) has generally slower kinetics at most steps than those reported for other myosin II isoforms. The most striking differences in the kinetics of NMIIB compared with that of muscle myosin isoforms are that it has the highest ADP affinity reported so far, which is, surprisingly, further elevated by actin, and that its ADP release kinetics is only about three times faster than the steady-state actin-activated MgATPase rate. This implies that the strongly actin-bound states can constitute a rather significant proportion of myosin molecules during steady-state ATP hydrolysis and that physiological changes in ADP concentration can profoundly affect the mechanical performance of this myosin and thus have consequences in exerting its cellular function.

EXPERIMENTAL PROCEDURES

Cloning, Expression, and Purification of the NMIIB S1 Protein—cDNA for human NMIIB was truncated at amino acid 843 to create an S1-like fragment and subcloned into baculovirus transfer vector pVL1392 (Invitrogen). Nucleotides (GACTACAAGGACGACGATGATAAG) encoding a FLAG epitope (DYKDDDDK) followed by a stop codon were appended to the C terminus of NMIIB S1 to aid purification. The complete nucleotide sequence of the resulting vector was confirmed by double-stranded DNA sequencing. The NMIIB gene can be alternatively spliced at both loops 1 and 2 in the motor domain to create longer loops (12). We have expressed a version that contains the unspliced (non-inserted) version at each loop. The myosin heavy chain fragment was coexpressed with essential and regulatory light chains (5). The expressed NMIIB S1 protein was purified as previously described (13).

Actin from rabbit skeletal muscle was prepared (14) and pyrene-labeled as described (15). Mant-ATP and mant-ADP were purchased from Molecular Probes, Inc. (Eugene, OR). Other reagents were from Sigma.

Steady-state Actin-activated ATPase Measurements—Steady-state ATPase activities were measured by an NADH-coupled assay at 25 °C in buffer containing 10 mM MOPS (pH 7.0), 2 mM $MgCl_2$, 0.15 mM EGTA, 1 mM ATP, 40 units/ml lactate dehydrogenase, 200 units/ml pyruvate kinase, 1 mM phosphoenolpyruvate, and 200 μM NADH. Changes in A_{340} (ϵ = 6220 M^{-1} cm^{-1}) were followed in a Beckman DU640 spectrophotometer.

Stopped-flow Experiments—Unless stated otherwise, all stopped-flow measurements were done in an SF-2001 stopped-flow apparatus (KinTek Corp., Austin, TX) at 25 °C in buffer comprising 25 mM MOPS (pH 7.0), 5 mM $MgCl_2$, 100 mM KCl, and 0.1 mM EGTA. Tryptophan fluorescence was excited at 295 nm, and emission was selected with a band-pass filter having a peak in transmittance at 347 nm. Pyrene-

* The costs of publication of this article were defrayed in part by the payment of page charges. This article must therefore be hereby marked "*advertisement*" in accordance with 18 U.S.C. Section 1734 solely to indicate this fact.

‡ Both authors contributed equally to this work.

§ To whom correspondence should be addressed: Lab. of Molecular Cardiology, NHLBI, NIH, Bldg. 10, Rm. 8N202, Bethesda, MD 20892-1762. Tel.: 301-496-6887; Fax: 301-402-1542; E-mail: sellersj@nhlbi.nih.gov.

[1] The abbreviations used are: NMIIA, NMIIB, and NMIIC, non-muscle myosins IIA, IIB, and IIC, respectively; S1, subfragment-1; mant-, *N*-methylanthraniloyl-; MOPS, 4-morpholinepropanesulfonic acid; MDCC-PBP, *N*-[2-(1-maleimidyl)ethyl]-7-(diethylamino)coumarin 3-carboxamide-labeled A197C point mutant bacterial phosphate-binding protein.

labeled actin was excited at 365 nm, and the emitted light was selected using a 400-nm long-pass cutoff filter. Mant-ATP and mant-ADP were excited via energy transfer from tryptophan (295 nm excitation), and the emitted light was selected using a 400-nm long-pass cutoff filter. Concentrations stated throughout this study refer to cuvette concentrations unless otherwise indicated.

The kinetics of P_i release from NMIIB S1 or acto-NMIIB S1 was followed using a mutant bacterial phosphate-binding protein covalently labeled with *N*-[2-(1-maleimidyl)ethyl]-7-(diethylamino)coumarin 3-carboxamide (MDCC-PBP) (16). The fluorophore was excited at 436 nm (6-nm bandwidth), and the emitted light was selected through a 450-nm long-pass cutoff filter. Experiments were done in sequential mixing mode in the SF-2001 stopped-flow apparatus at 25 °C in buffer comprising 4 mM MOPS (pH 7.1), 2 mM $MgCl_2$, and KCl at different concentrations (0, 50 or 100 mM). All syringes contained 3 μM MDCC-PBP. All solutions were preincubated with a "phosphate mop" consisting of 0.02 units/ml purine-nucleoside phosphorylase and 0.1 mM 7-methylguanosine to remove P_i contamination. Actin filaments were stabilized by addition of an equimolar amount of phalloidin (Calbiochem), which also abolished the background signal arising from breakdown of ATP by actin.

Quenched-flow Experiments—Chemical quench measurements were performed using an RQF-3 quenched-flow apparatus (KinTek Corp.). Samples (15 μl) of S1 or acto-S1 were mixed with an equal volume of ATP containing [γ-^{32}P]ATP. After aging in the delay line, reactions were stopped by mixing with a solution containing 22% trichloroacetic acid and 1 mM KH_2PO_4 (to approximately one-third of the total volume). P_i was extracted from the samples immediately by adding 250 μl of 5% ammonium molybdate, 650 μl of 0.6 M H_2SO_4, 0.3% silicotungstic acid, 0.6 mM potassium P_i, and 1 ml of a 1:1 mixture of isobutyl alcohol and toluene. After vortexing for 30 s and a 1-min incubation at room temperature, 0.5 ml of the organic phase was mixed with scintillation mixture and counted. Total radioactivity in the samples was determined by direct counting of the [γ-^{32}P]ATP solution. Measurements were carried out at 25 °C in buffer comprising 8 mM MOPS (pH 7.1), 1 mM $MgCl_2$, and 0.1 mM EGTA. In the absence of actin, addition of 100 mM KCl was required for stability of NMIIB S1. When necessary, ADP contamination was removed from NMIIB S1 samples by incubation with 0.01/ml apyrase (Sigma) at 25 °C for 30 min. Column-purified ATP was used in the experiments to minimize ADP contamination (17).

Data Analysis and Modeling—Fitting of the experimental traces was performed using the KinTek software, SigmaPlot 2001, and Origin 6.0 (Microcal Software). Kinetic simulations were performed with Gepasi Version 3.21 (Pedro Mendes, Virginia Bioinformatics Institute). Means ± S.D. reported for the kinetic constants are those of three to four separate rounds of experiment.

RESULTS

Preparation and Steady-state Characterization of NMIIB S1—An NMIIB S1 heavy chain fragment containing 843 amino acids from its amino terminus was coexpressed along with regulatory and essential light chains in the baculovirus system. The resulting NMIIB S1 was purified from Sf9 cell extracts using FLAG affinity chromatography. More than 10 mg of protein could be prepared from ~4×10^9 cells. The expressed S1 had a basal MgATPase activity of 0.007 ± 0.001 s^{-1} in the absence of actin. MgATPase activities of S1 at various actin concentrations were fitted to the Michaelis-Menten equation, giving V_{max} = 0.13 ± 0.01 s^{-1} and K_{ATPase} ~ 59 μM at 25 °C (Fig. 1). This is one of the lowest V_{max} values recorded for any myosin.

We used a kinetic model of the acto-NMIIB S1 ATPase cycle similar to those used in recent studies of other myosins (18, 19). Throughout this work, the numbering of kinetic steps refers to Scheme 1.

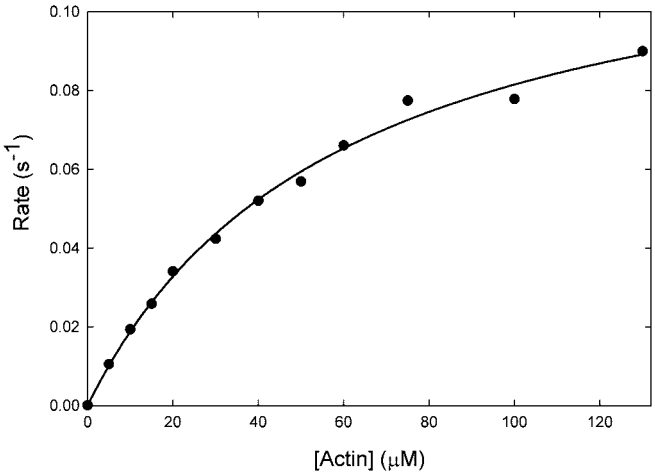

FIG. 1. **Steady-state actin-activated MgATPase activity of NMIIB S1.** The MgATPase activities of NMIIB S1 in the absence of actin and of actin alone were subtracted from the experimentally measured rates and plotted. The curve is a fit to a hyperbolic Michaelis-Menten equation with V_{max} = 0.13 ± 0.01 s^{-1} and K_{ATPase} = 59 ± 3 μM.

In this model, the actin-associated pathway of ATP binding, hydrolysis, and product release is shown in the upper line (AM stands for actomyosin), whereas the lower line represents the same events when myosin (M) is dissociated from actin (A). The main flux pathway of the reaction is highlighted in boldface. The equilibrium constants throughout this work are expressed as viewed in a direction processing to the right in Scheme 1, and those between actin-associated and actin-dissociated states going in the dissociation direction. Similarly, rate constants have positive indices in these directions. ATP binding was modeled as a two-step reaction consisting of a second-order collision step (K_1 or K_1') and a subsequent isomerization (K_2 or K_2') that becomes rate-limiting at high ATP concentrations. Although ADP binding (and dissociation) has been shown to consist of similar events (20), we consider it as a single step (K_5 or K_5') for simplicity because the substeps were not resolved in the course of this study. The same holds for the ATP hydrolysis step (K_3 or K_3') that has been resolved to a conformational transition and the actual chemical step (21), with phosphate release (K_4 or K_4') probably being similar to it in this respect.

Actin Binding—As shown for other myosins (22), binding of NMIIB S1 or NMIIB S1·ADP to pyrene-labeled actin decreases pyrene fluorescence (Schemes 2 and Scheme 3),

$$\mathrm{M} + \mathrm{A}^* \underset{k_6}{\overset{k_{-6}}{\rightleftharpoons}} \mathrm{AM}$$

SCHEME 2

$$\mathrm{M \cdot ADP} + \mathrm{A}^* \underset{k_{10}}{\overset{k_{-10}}{\rightleftharpoons}} \mathrm{AM{\cdot}ADP}$$

SCHEME 3

where A* represents the high fluorescence state of actin. The time course of the decrease in pyrene fluorescence upon rapidly

$$\begin{array}{ccccccccccc}
 & & \boldsymbol{K_1'} & & \boldsymbol{K_2'} & & K_3' & & \boldsymbol{K_4'} & & \boldsymbol{K_5'} \\
\mathbf{AM + ATP} & \rightleftharpoons & \mathbf{AM(ATP)} & \rightleftharpoons & \mathbf{AM \cdot ATP} & \rightleftharpoons & \mathbf{AM \cdot ADP \cdot P_i} & \rightleftharpoons & \mathbf{AM \cdot ADP} & \rightleftharpoons & \mathbf{AM} \\
\Downarrow K_6 & & \Downarrow K_7 & & \Downarrow \boldsymbol{K_8} & & \Downarrow \boldsymbol{K_9} & & \Downarrow K_{10} & & \Downarrow K_6 \\
\mathrm{M + ATP} & \underset{}{\overset{K_1}{\rightleftharpoons}} & \mathrm{M(ATP)} & \underset{}{\overset{K_2}{\rightleftharpoons}} & \mathbf{M \cdot ATP} & \underset{}{\overset{\boldsymbol{K_3}}{\rightleftharpoons}} & \mathbf{M \cdot ADP \cdot P_i} & \underset{}{\overset{K_4}{\rightleftharpoons}} & \mathrm{M \cdot ADP} & \underset{}{\overset{K_5}{\rightleftharpoons}} & \mathrm{M}
\end{array}$$

SCHEME 1

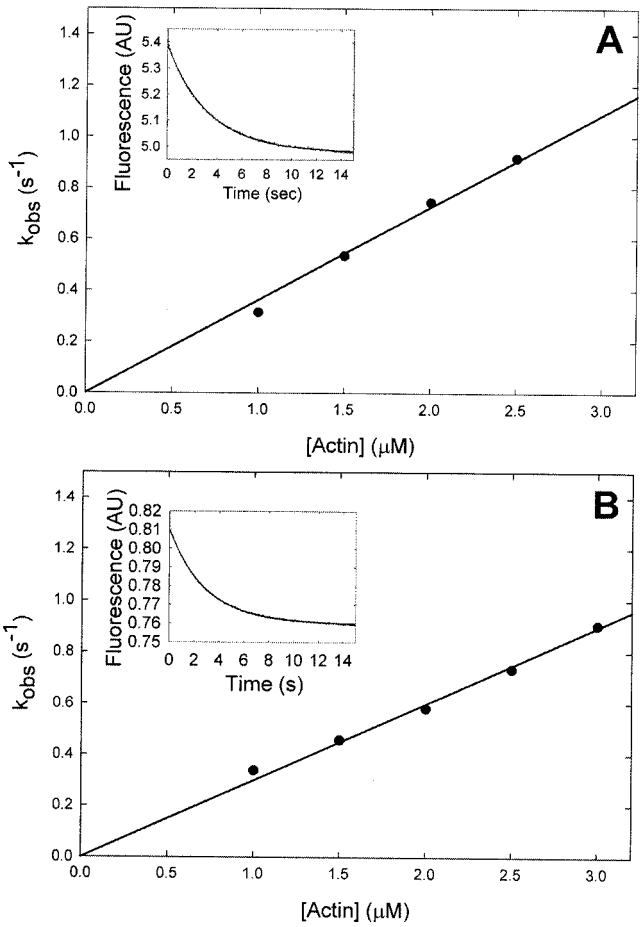

FIG. 2. **Kinetics of NMIIB S1 binding to pyrene-labeled actin filaments.** *A*, dependence of k_{obs} on actin concentration. The *solid line* is a linear fit of the data set that gave an apparent second-order rate constant (k_{-6}) of 0.36 ± 0.04 μM^{-1} s^{-1}. *Inset*, an averaged time course of pyrene fluorescence quenching after mixing 1 μM pyrene-labeled actin with 0.1 μM NMIIB S1. Typically, at least three transients were averaged for fitting to a single exponential function (*solid line*, k_{obs} = 0.30 s^{-1} in the trace shown). *B*, dependence of the observed binding rate constant on actin concentration in the presence of ADP. The *solid line* is a linear fit of the data set resulting in an apparent second-order rate constant (k_{-10}) of 0.30 μM^{-1} s^{-1} in the example shown. *Inset*, an averaged time course of fluorescence quenching after mixing 1 μM pyrene-labeled actin with 0.1 μM NMIIB-S1 and 2.5 μM ADP, yielding k_{obs} = 0.34 s^{-1}. *AU*, arbitrary units.

mixing with NMIIB S1 in a stopped-flow spectrofluorometer could be fitted to a single exponential equation to yield a pseudo first-order rate constant, k_{obs} (Fig. 2*A*, *inset*). The dependence of k_{obs} on actin concentration was linear, and its slope gave an apparent second-order rate constant (k_{-6}) of 0.36 ± 0.04 μM^{-1} s^{-1} (Fig. 2*A*). This is slower by a factor of 3 compared with that observed for smooth muscle myosin (23) and slower by a factor of >10 compared with those observed for most other classes of myosin (1). Similarly, the binding of NMIIB S1·ADP to actin could be measured (Fig. 2*B*), where an apparent second-order rate constant (k_{-10}) of 0.26 ± 0.11 μM^{-1} s^{-1} was obtained. These results are summarized in Table I.

The actin affinity of NMIIB S1 (K_6) can be determined by measuring the amplitude change in pyrene fluorescence occurring upon the ATP-induced dissociation of NMIIB S1·pyrene-labeled actin as a function of NMIIB S1 concentration (22). In these experiments, concentrations before mixing are given because these are relevant in terms of calculation of the equilibrium parameters. The fluorescence amplitude was measured on mixing 5 μM ATP with a pre-mix of 15 nM pyrene-labeled actin and various concentrations of NMIIB S1. Fitting the data to a quadratic binding equation revealed a dissociation constant (K_6) of 3.2 ± 0.3 nM (Fig. 3*A*) (24). Using the same method, the affinity of NMIIB S1·ADP for actin was also measured, giving K_{10} = 1.2 ± 0.4 nM (Fig. 3*B*). Hyperbolic fittings of these same data sets gave K_6 = 10 nM and K_{10} = 11 nM. Because the dissociation constants are rather low compared with the actin and S1 concentrations used, the determined parameters are likely to represent upper limits for K_6 and K_{10}. Nevertheless, the results clearly reveal that ADP does not dramatically affect the affinity of NMIIB S1 for actin (Table I). From the equilibrium dissociation constant and the on-rate constant, dissociation rate constants of 0.0012 s^{-1} (k_6) and 0.0003 s^{-1} (k_{10}) could be calculated (Table I).

ATP-induced Dissociation of Acto-NMIIB S1—Scheme 4 shows that the fluorescence of pyrene-labeled actin can also be used to monitor the kinetics of the formation of the weak actin-binding states of myosin upon ATP binding.

$$\mathrm{AM} + \mathrm{ATP} \underset{}{\overset{K_1'}{\rightleftharpoons}} \mathrm{AM(ATP)} \underset{k_{+2}'}{\overset{k_{-2}'}{\rightleftharpoons}} \mathrm{A^*M \cdot ATP}$$

SCHEME 4

Rapidly mixing MgATP with pyrene-labeled acto-NMIIB S1 causes an increase in fluorescence levels approaching that of pyrene-labeled actin alone. The time courses of the mixing experiments followed single exponential kinetics, and a plot of the observed rate constant of increase *versus* MgATP concentration was hyperbolic (Fig. 4*A*). In the ATP concentration range examined (up to 2.5 mM), the observed rate constant saturated at >150 s^{-1} with a half-maximum above 400 μM ATP. The apparent second-order association rate constant for MgATP binding to pyrene-labeled acto-NMIIB S1 ($K_1'k_2'$) obtained from the initial slope of the plot at low ATP concentrations was 0.40 ± 0.11 μM^{-1} s^{-1} (average of two experiments) (Fig. 4*B*).

The fluorescent nucleotide mant-ATP increased its fluorescence upon binding to acto-NMIIB S1 (Fig. 4*C*), as has been shown to occur for other myosins. The fluorescence increase observed when mant-ATP was mixed with acto-NMIIB S1 could be fitted to a single exponential equation to determine the observed rate constant. A plot of k_{obs} *versus* mant-ATP concentration is linear and gives an apparent second-order rate constant of 0.24 ± 0.02 μM^{-1} s^{-1}, which is in reasonable agreement with the value for $K_1'k_2'$ measured above for the population of the weakly bound states.

ATP Binding—The binding of ATP to myosin in the absence of actin was followed in two ways. In the first case, the change in tryptophan fluorescence that occurs in NMIIB S1 upon mixing with ATP, similar to several other myosin isoforms (20, 25, 26), was monitored. In the second case, the fluorescence increase in mant-ATP upon binding to myosin was measured. This reaction was modeled according to Scheme 5.

$$\mathrm{M} + \mathrm{ATP} \underset{}{\overset{K_1}{\rightleftharpoons}} \mathrm{M(ATP)} \overset{k_2}{\longrightarrow} \mathrm{M \cdot ATP^*}$$

SCHEME 5

NMIIB S1 showed a 8–10% increase in tryptophan fluorescence upon mixing with ATP that could be fitted to a single exponential (Fig. 5*A*, *inset*). The observed rate constant increased hyperbolically with ATP concentration and saturated at a rate of 16.5 ± 0.2 s^{-1} with a half-saturation at 17.5 μM ATP (Fig. 5*A*). Thus, at high ATP concentrations, the rate of fluorescence enhancement was limited by the ATP hydrolysis step, and its maximal rate reports the rate of ATP hydrolysis (Scheme 1, k_{+3} + k_{-3}). At low ATP concentrations, the ob-

TABLE I
Kinetic parameters of the acto-NMIIB-S1 ATPase cycle

All experiments were done at 25 °C. Equilibrium constants are expressed as viewed to the right side or downwards in Scheme 1. Reported S.E. values are those of three to four different rounds of experiments.

Parameter	Signal or calculation	Value
Steady-state ATPase activity[a]		
Basal ATPase	NADH-coupled assay	$0.007 \pm 0.001\ s^{-1}$
V_{max}	NADH-coupled assay	$0.13 \pm 0.01\ s^{-1}$
K_{ATPase}	NADH-coupled assay	$59 \pm 3\ \mu M$
ATP binding		
K_1k_2	Mant-ATP	$0.65 \pm 0.06\ \mu M^{-1}\ s^{-1}$
K_1k_2	Tryptophan	$0.72 \pm 0.04\ \mu M^{-1}\ s^{-1}$
$K_1'k_2'$	Mant-ATP	$0.24 \pm 0.02\ \mu M^{-1}\ s^{-1}$
$K_1'k_2'$	Pyrene-actin	$0.40 \pm 0.11\ \mu M^{-1}\ s^{-1}$
$1/K_1'$	Pyrene-actin	$> 400\ \mu M$
k_2'	Pyrene-actin	$> 150\ s^{-1}$
ADP binding		
k_{-5}	Mant-ADP	$0.81 \pm 0.23\ \mu M^{-1}\ s^{-1}$
k_5	Mant-ADP[b]	$0.58 \pm 0.13\ s^{-1}$
k_5	Mant-ADP[c]	$0.48 \pm 0.11\ s^{-1}$
K_5	k_5/k_{-5}	$0.65 \pm 0.3\ \mu M$
k_{-5}'	Mant-ADP	$2.41 \pm 0.13\ \mu M^{-1}\ s^{-1}$
k_5'	Mant-ADP[b]	$0.35 \pm 0.03\ s^{-1}$
k_5'	Mant-ADP[c]	$0.38 \pm 0.09\ s^{-1}$
K_5'	k_5'/k_{-5}'	$0.15 \pm 0.03\ \mu M$
K_5'	Pyrene-actin[d]	$0.11 \pm 0.03\ \mu M$
K_5'	Mant-ADP[d]	$0.017 \pm 0.013\ \mu M$
K_5'/K_5		0.2
ATP hydrolysis		
$k_3 + k_{-3}$	Tryptophan	$16.5 \pm 0.2\ s^{-1}$
$k_3 + k_{-3}$	Quenched-flow	$19.8 \pm 1.0\ s^{-1}$
K_3	Quenched-flow	0.9 ± 0.2
k_3	$K_3(k_3 + k_{-3})/(1 + K_3)$	$9 \pm 3\ s^{-1}$
k_{-3}	k_3/K_3	$10 \pm 3\ s^{-1}$
Phosphate release[e]		
k_4	MDCC-PBP	$0.007 \pm 0.001\ s^{-1}$
K_9	MDCC-PBP	$>50\ \mu M$
Actin binding		
k_{-6}	Pyrene-actin	$0.36 \pm 0.04\ \mu M^{-1}\ s^{-1}$
K_6	Pyrene-actin[d]	$0.0032 \pm 0.003\ \mu M$
k_6	K_6k_{-6}	$0.0012 \pm 0.0003\ s^{-1}$
k_{-10}	Pyrene-actin	$0.26 \pm 0.11\ \mu M^{-1}\ s^{-1}$
K_{10}	Pyrene-actin[d]	$0.0012 \pm 0.0004\ \mu M$
k_{10}	$K_{10}k_{-10}$	$0.0003 \pm 0.0001\ s^{-1}$
K_{10}/K_6		≈ 0.4

[a] At 0 mM KCl.
[b] From the *y* intercept of the k_{obs} *versus* [mant-ADP] plot.
[c] From the ATP chasing experiment.
[d] From amplitude data.
[e] At 50 mM KCl.

served rate was limited by the ATP binding process; therefore, it was linearly dependent upon ATP concentration up to 5 μM ATP, and the slope gave an apparent second-order rate constant (K_1k_2) of $0.72 \pm 0.04\ \mu M^{-1}\ s^{-1}$ (Fig. 5*B*). Using mant-ATP as a substrate, a similar association rate constant ($0.65 \pm 0.06\ \mu M^{-1}\ s^{-1}$) was obtained (Fig. 5*C*).

ATP Hydrolysis—The kinetics of ATP hydrolysis by NMIIB S1 and acto-NMIIB S1 was measured by chemical quench experiments. Similar to other myosins examined, an initial burst in P_i production was observed upon mixing NMIIB S1 or acto-NMIIB S1 with excess ATP (Fig. 6*A*), indicating that ATP hydrolysis occurs before the rate-limiting step of the process. The burst phase was exponential with $k_{obs} = 19.8 \pm 1.0\ s^{-1}$ in the absence of actin. The k_{obs} of the burst was identical when NMIIB S1 was mixed with 50 and 100 μM ATP, indicating that it is not limited by the nucleotide binding process. Its value is in good agreement with the results of the stopped-flow experiments monitoring the enhancement of tryptophan fluorescence (see above), where the rate saturated at $16.5\ s^{-1}$. In the presence of actin, the k_{obs} of the burst was $11.0 \pm 0.6\ s^{-1}$ at 50 μM ATP (Fig. 6*A*). The lower value may result from nucleotide binding being still rate-limiting at this ATP concentration, because the ATP on-rate of acto-NMIIB S1 is significantly slower than that of NMIIB S1 (see above.) The burst was followed by a linear steady-state phase of ATP hydrolysis, where the extent of rate enhancement caused by 20 μM actin was similar to the results of the steady-state ATPase measurements (data not shown).

The amplitude of the initial P_i burst ($n_{P_i}/n_{NMIIB\ S1}$) can be used to calculate the equilibrium constant of the hydrolysis step (K_3). This amplitude was unusually low in both the absence and presence of actin (0.42 ± 0.03 and 0.44 ± 0.05, respectively), indicating that the hydrolysis step is more reversible in NMIIB S1 than in any other myosin isoform examined. Because the accuracy of these results depends on protein concentration measurements and is also affected by the amount of nonfunctional myosin heads in the preparation, we performed single turnover ATP hydrolysis experiments that provide an independent measure of K_3. In these experiments, the fraction of ATP hydrolyzed during the initial process limited by nucleotide binding gives the burst amplitude. Although reactions did not take place under pseudo first-order conditions (NMIIB S1 was at only ~2–3-fold molar excess over ATP), double exponential fits gave reasonable amplitude data for the burst and slow phases (Fig. 6*B*). The burst amplitudes (between 0.41 and 0.56) were in good agreement with the results

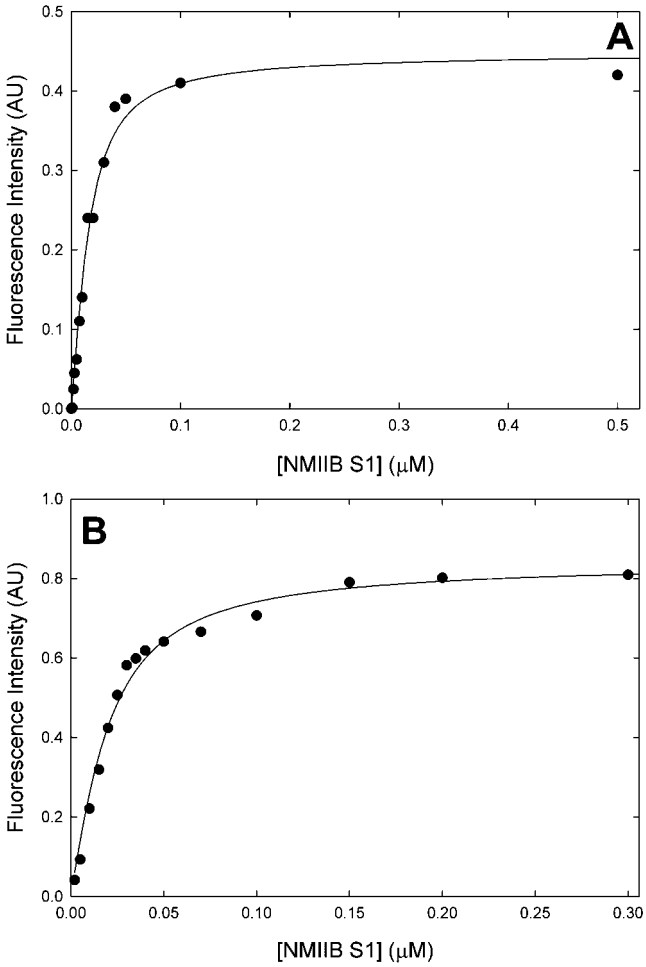

FIG. 3. **Equilibrium binding of NMIIB S1 and NMIIB S1·ADP to pyrene-labeled actin filaments.** *A*, various concentrations of NMIIB S1 were mixed with 15 nM pyrene-labeled actin and allowed to reach equilibrium prior to mixing with 5 μM ATP in the stopped-flow apparatus (premixing concentrations are indicated in these experiments). The amplitude of the pyrene fluorescence increase was measured and plotted as a function of NMIIB S1 concentration. The *solid line* is a quadratic fit, yielding K_6 = 3.2 ± 0.3 nM. *B*, shown are the results of a similar experiment, except that acto-NMIIB S1 and 5 μM ADP were mixed with 50 μM ATP. The fitted data gave a value of 1.2 ± 0.4 nM for K_{10}. *AU*, arbitrary units.

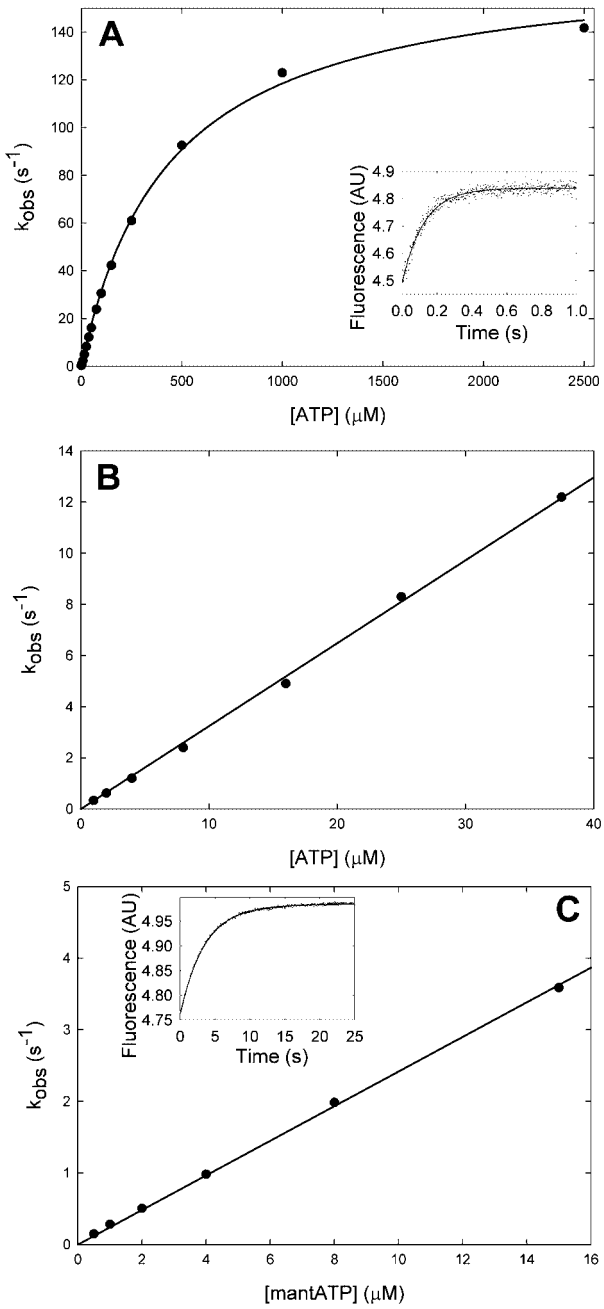

FIG. 4. **ATP-induced dissociation of acto-NMIIB S1 and binding of mant-ATP to acto-NMIIB S1.** *A*, dependence of k_{obs} on ATP concentration when mixing 0.04 μM pyrene-acto-NMIIB S1 with ATP. The *solid line* is a fit to a hyperbola with a maximal rate of 171 s^{-1}. The concentration of ATP at the half-maximal rate was 439 μM in the example shown. *Inset*, an averaged time course of the pyrene fluorescence increase after mixing 0.04 μM pyrene-labeled acto-NMIIB S1 with 50 μM ATP (k_{obs} = 16.8 s^{-1} in the example shown). *B*, k_{obs} *versus* ATP concentration at low concentrations of ATP. The deduced second-order rate constant ($K_1'k_2'$) was 0.32 μM^{-1} s^{-1} in the example shown. *C*, dependence of k_{obs} of mant-ATP binding to 0.05 μM acto-NMIIB S1 on mant-ATP concentration. The deduced second-order rate constant ($K_1'k_2'$) was 0.24 μM^{-1} s^{-1} in the example shown. *Inset*, mant fluorescence increase upon mixing 0.05 μM acto-NMIIB S1 with 1 μM mant-ATP. The *solid line* shows the best single exponential fit, which gave an observed rate constant of 0.28 s^{-1}. *AU*, arbitrary units.

of the multiple turnover experiments described. The equilibrium constant of the hydrolysis step calculated using the averages of the burst amplitudes obtained by different methods ($K_3 = A/(1 - A)$, where A is the burst amplitude) was 0.9 ± 0.3 in the absence and 0.9 ± 0.1 in the presence of 20 μM actin. The ATP hydrolysis step is fairly reversible in all myosins investigated (*e.g.* K_3 = 9 in skeletal muscle myosin) (1), but this is the lowest K_3 value ever reported. Myosin I isoforms from *Acanthamoeba* have similarly low K_3 values (~1.5) (27). Because the observed ATP hydrolysis step has been shown to be composed of a conformational transition in the protein and of the actual chemical step (21, 28), a change in any of these steps can result in the low K_3 value reported here.

ADP Binding and Dissociation—The binding of mant-ADP to NMIIB S1 was also monitored by fluorescence (Fig. 7*A*, *inset*). The k_{obs} was linearly dependent on mant-ADP concentration over the range tested (Fig. 7*A*). The slope gave a second-order rate constant (k_{-5}) of 0.81 ± 0.23 μM^{-1} s^{-1}. The ordinate intercepts reflect the dissociation rate constant (k_5), which was determined to be 0.58 ± 0.13 s^{-1}. A similar linear dependence of k_{obs} on mant-ADP concentration was observed when the nucleotide was mixed with acto-NMIIB S1 (Fig. 7*B*). Here, the apparent second-order rate constant (k_{-5}') was determined to be 2.41 ± 0.13 μM^{-1} s^{-1}. The ordinate intercept gives k_5' = 0.35 ± 0.03 s^{-1}. This value for the ADP release from acto-NMIIB S1 is surprisingly low. Most myosin II class molecules, when bound to actin, have an ADP release rate that is much

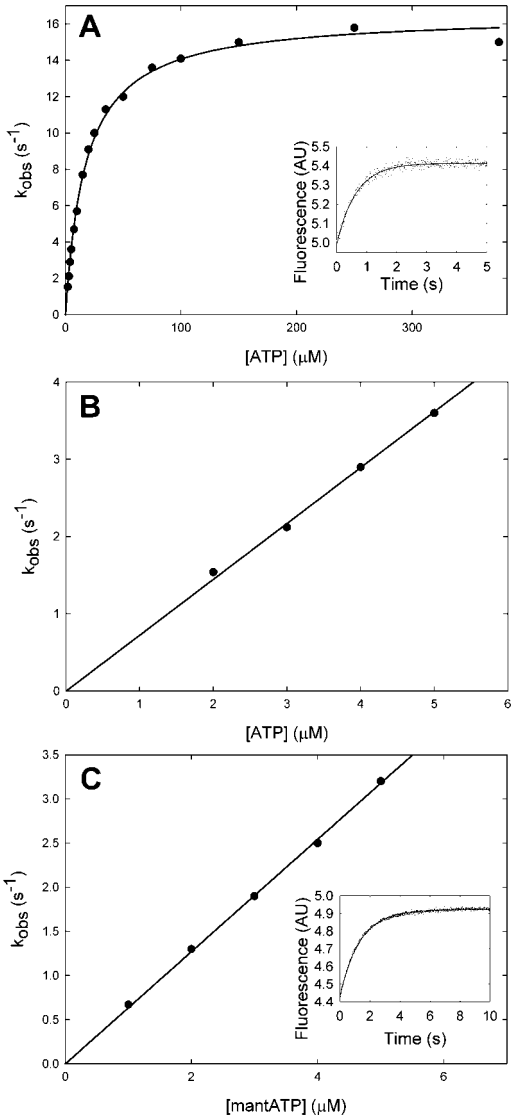

FIG. 5. **ATP and mant-ATP binding to NMIIB S1.** *A*, dependence of k_{obs} of tryptophan fluorescence increase on ATP concentration. The *solid line* is a hyperbolic fit to the data, yielding a maximal observed rate constant of 16.5 ± 0.2 s^{-1} (corresponding to the rate constants of the hydrolysis step, $k_3 + k_{-3}$) and a concentration of ATP at half-maximal saturation of the rate at 17.5 μM ATP. *Inset*, an averaged time course of the tryptophan fluorescence increase upon mixing 0.2 μM NMIIB S1 with 4 μM ATP. The *solid line* is a single exponential fit with k_{obs} = 1.5 s^{-1}. *B*, k_{obs} *versus* low ATP concentrations. The deduced second-order rate constant (K_1k_2) was 0.72 μM^{-1} s^{-1} in the example shown. *C*, dependence of k_{obs} of mant-ATP binding to NMIIB S1 on mant-ATP concentration. The deduced second-order rate constant (K_1k_2) was 0.64 μM^{-1} s^{-1} in the example shown. *Inset*, averaged time course of the mant fluorescence increase upon mixing 0.1 μM NMIIB S1 with 1 μM mant-ATP. The *solid line* is a single exponential fit with k_{obs} = 0.75 s^{-1}. *AU*, arbitrary units.

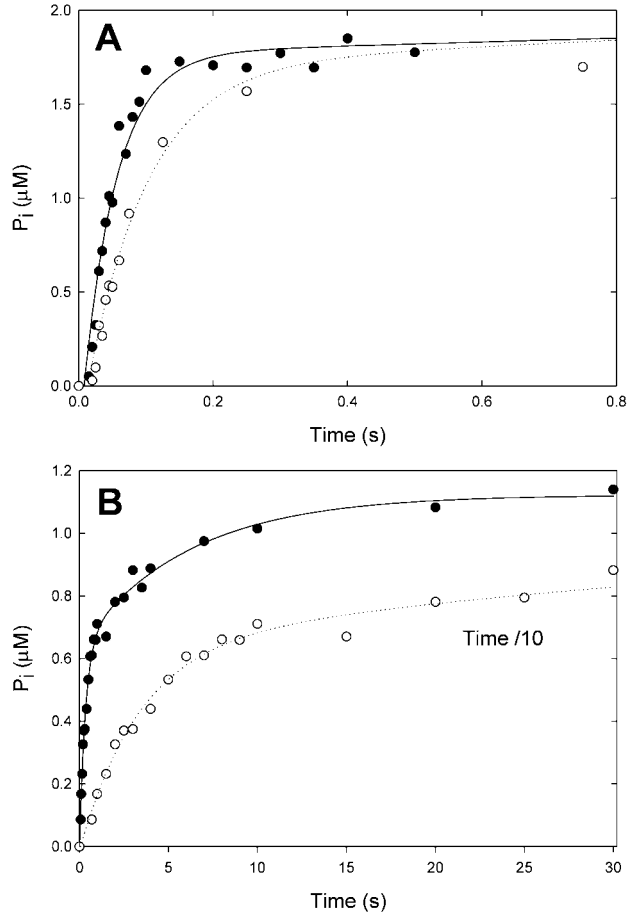

FIG. 6. **Kinetics of ATP hydrolysis measured by quenched flow.** *A*, initial P_i burst and steady-state ATP hydrolysis by NMIIB S1 and acto-NMIIB S1. 50 μM ATP was mixed with either 4 μM NMIIB S1 (●) or 3.7 μM NMIIB S1 and 20 μM actin (○). Data were fitted to single exponentials with a linear slope. The amplitude of the initial burst was 0.4 mol of P_i/mol of NMIIB S1 in the absence of actin, and the k_{obs} of ATP hydrolysis ($k_3 + k_{-3}$) was 18.8 s^{-1} in the example shown. In the presence of actin, the burst had an amplitude of 0.44 mol of P_i/mol of S1 and k_{obs} = 11.0 s^{-1} in the trace shown. *B*, kinetics of ATP hydrolysis during a single turnover. Shown is a time course of the reaction of 3.7 μM NMIIB S1 plus 20 μM actin mixed with 1.5 μM ATP. ●, data are plotted on a 30-s time scale; ○, the same data set is plotted on a 3-s time scale. Double exponential approximation proved applicable even though the reaction did not take place under pseudo first-order conditions. The fit shown had amplitudes of 0.66 and 0.48 μM for the fast and slow phases, respectively.

higher than the steady-state actin-activated MgATPase rate (1), but the rate of ADP release from acto-NMIIB S1 is only about two to three times higher than the steady-state ATPase rate. Therefore, a different means to determine its value was used. The decrease in fluorescence upon dissociation of mant-ADP from either NMIIB S1 (Fig. 8*A*) or acto-NMIIB S1 (Fig. 8*B*) upon mixing with excess ATP was measured to yield independent values of k_5 and k_5'. Fitting the transients to single exponentials gave rates of 0.48 ± 0.11 and 0.38 ± 0.09 s^{-1} for the dissociation of mant-ATP from NMIIB S1 alone and acto-NMIIB S1, respectively, in good agreement with the values determined in Fig. 7 from the ordinate intercepts.

The affinity of acto-NMIIB S1 for ADP was measured by premixing 0.04 μM pyrene-labeled acto-NMIIB S1 with various concentrations of ADP in one syringe of the stopped-flow apparatus and then rapidly mixing with 100 μM ATP (premixing concentrations) (Fig. 9*A*, *inset*). The resulting transients were fitted to a single exponential in the absence of ADP and to double exponentials in the presence of ADP. The rate constant of the fast phase was ~40 s^{-1} and corresponded to ATP-induced dissociation of acto-NMIIB S1 in the absence of nucleotide (see above). The relative amplitude of this phase reflected the portion of acto-NMIIB S1 free of bound nucleotide. The rate constant of the slow phase was 0.34 s^{-1} and was limited by ADP dissociation, which must precede ATP binding. The relative amplitude of this slow phase represented the fraction of acto-NMIIB S1 molecules that were bound to ADP. A plot of the relative amplitude of the slow phase (*i.e.* $A_{slow}/(A_{fast} + A_{slow})$) *versus* ADP concentration was fitted to a quadratic equation to give a dissociation constant (K_5') of 110 ± 30 nM (Fig. 9*B*), in good agreement with the K_5' value calculated from the on- and

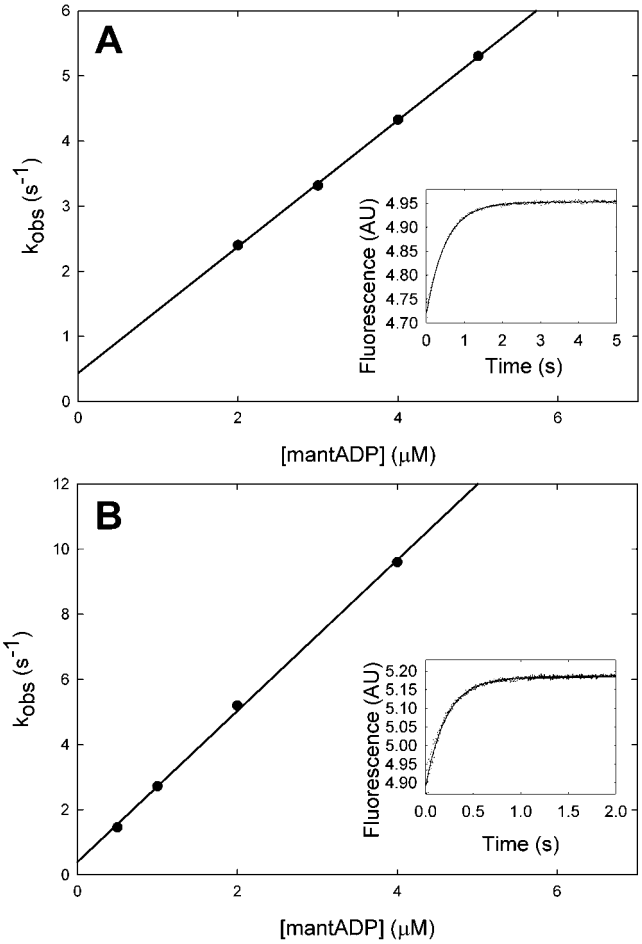

FIG. 7. **Mant-ADP binding to NMIIB-S1 and acto-NMIIB-S1.** *A*, dependence of k_{obs} of mant-ADP binding to NMIIB S1 on mant-ADP concentration. The deduced second-order rate constant (k_{-5}) was 0.97 μM^{-1} s^{-1} with a *y intercept* (k_5) of 0.44 s^{-1} in the example shown. *Inset*, averaged time course of the mant-ADP fluorescence increase upon mixing 0.2 μM NMIIB S1 with 2 μM mant-ADP. The *solid line* is the best single exponential fit with k_{obs} = 1.97 s^{-1}. *B*, dependence of k_{obs} of mant-ADP binding to acto-NMIIB S1 on mant-ADP concentration. The deduced second-order rate constant (k_{-5}') was 2.32 μM^{-1} s^{-1} with a *y intercept* (k_5') of 0.40 s^{-1} in the example shown. *Inset*, averaged time course of the mant-ADP fluorescence increase upon mixing 0.2 μM acto-NMIIB S1 with 2 μM mant-ADP. The *solid line* is the best single exponential fit with k_{obs} = 4.6 s^{-1}. *AU*, arbitrary units.

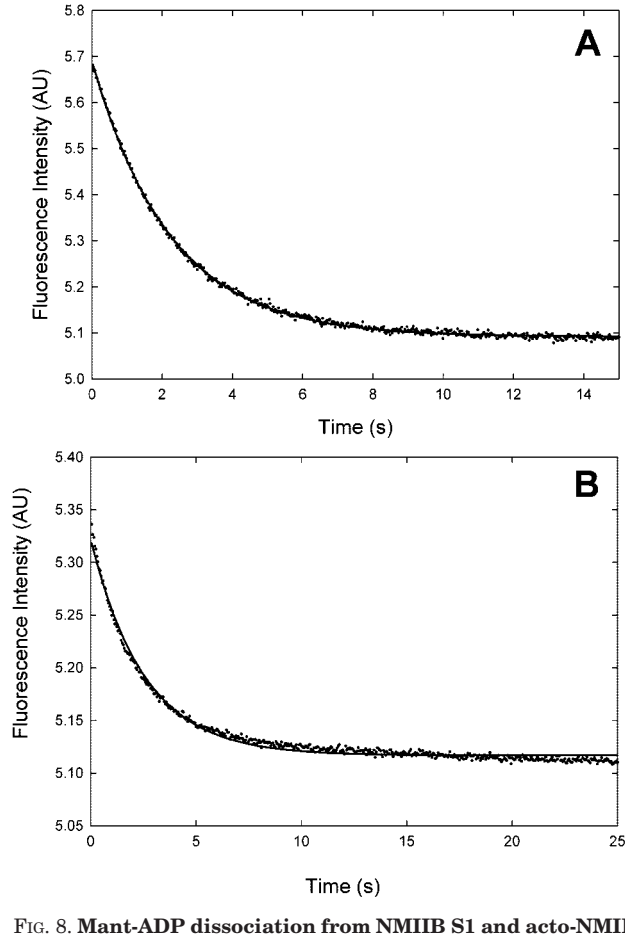

FIG. 8. **Mant-ADP dissociation from NMIIB S1 and acto-NMIIB S1.** *A*, averaged time course of the mant-ADP fluorescence decrease as mant-ADP was displaced from NMIIB S1 after mixing 0.2 μM NMIIB S1 plus 2 μM mant-ADP with 200 μM ATP. The *solid line* is the best single exponential fit, which gave an observed rate constant (k_5) of 0.45 s^{-1} in the example shown. *B*, averaged time course of the mant-ADP fluorescence decrease as mant-ADP was displaced from acto-NMIIB S1 after mixing 0.1 μM acto-NMIIB S1 plus 0.5 μM mant-ADP with 200 μM ATP. The *solid line* is the best single exponential fit, which gave an observed rate constant (k_5') of 0.40 s^{-1}. *AU*, arbitrary units.

off-rate constants (Table I). This reflects a very high affinity of NMIIB S1 for ADP in the presence of actin.

To confirm the high ADP affinity of acto-NMIIB S1, varying concentrations of stoichiometric acto-NMIIB S1 complexes were mixed with a constant concentration of 0.2 μM mant-ADP (Fig. 9*B*, *inset*). The dependence of the amplitude of the increase in mant-ADP fluorescence on acto-NMIIB S1 concentration (Fig. 9*B*) was analyzed similarly to the pyrene transients described above (except that here the post-mixing concentrations are relevant) and yielded a value of 17 ± 13 nM for K_5'. This value is lower by an order of magnitude even than those obtained by the other methods, and it contains a considerable error because of the tight binding. Nevertheless, this measurement also confirms that K_5' is unusually low.

Phosphate Release—P_i release was monitored using MDCC-PBP (16). When NMIIB S1 was mixed with ATP under single turnover conditions (2 μM protein and 1.5 μM ATP), the fluorescence increase could be fitted to a single exponential with k_{obs} = 0.007 ± 0.001 s^{-1} (trace not shown). This value is identical to the basal steady-state ATPase rate of NMIIB S1 and shows that phosphate release is rate-limiting in the absence of actin filaments. Nucleotide binding and hydrolysis are much faster processes even at the low ATP and protein concentrations used (see above).

To measure the kinetics of P_i release from the weakly actin-bound states of NMIIB S1, we performed double mixing stopped-flow experiments in which NMIIB S1 (0.7–2 μM) was premixed with ATP (0.5–1.5 μM) under single turnover conditions, incubated for 10 s in a delay line to allow sufficient time for ATP binding and hydrolysis, and then mixed with actin filaments at various concentrations with concomitant triggering of the record of the MDCC-PBP fluorescence signal. Single exponential transients with observed rate constants in the order of 0.010–0.015 s^{-1} were obtained throughout the actin concentration range examined (10–60 μM) (*e.g.* the one in Fig. 10). These values are lower than the steady-state actin-activated ATPase rates at the corresponding actin concentrations (*cf.* Fig. 1). The difference could be due to the fact that the steady-state assays were performed under very low ionic strength conditions (no KCl present), whereas in the stopped-flow experiments described here, at least 50 mM KCl had to be added to stabilize NMIIB S1 in a solution without actin or nucleotide. (There was no significant difference between the P_i release transients at 50 and 100 mM KCl.) To test this possibility, we measured the steady-state actin-activated ATPase activity of NMIIB S1 in 100 mM KCl. The amount of activation

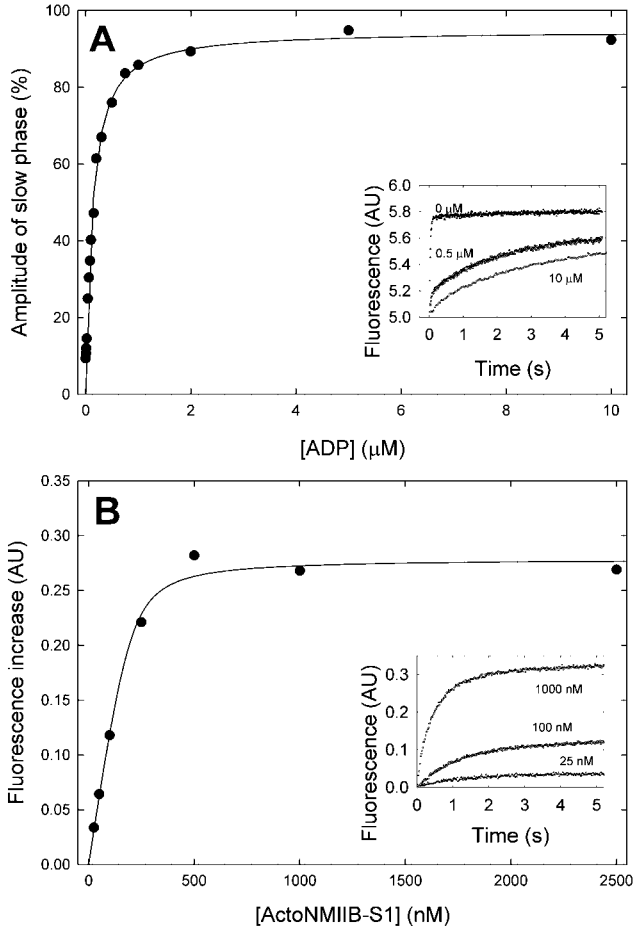

FIG. 9. **ADP affinity for acto-NMIIB S1.** *A*, 0.04 μM pyrene-acto-NMIIB-S1 was preinculated with various concentrations of ADP and mixed with 100 μM ATP (pre-mixing concentrations). Shown is the ADP dependence of the relative amplitude of the slow phase of the double exponential fit (*i.e.* $100\% \times A_{slow}/(A_{fast} + A_{slow})$). The data were fitted to a quadratic equation, yielding a value of 0.11 ± 0.03 μM for K_5' in the example shown. *Inset*, averaged time courses of the pyrene fluorescence increase upon mixing 0.04 μM pyrene-labeled acto-NMIIB S1 plus ADP (at the concentrations indicated) with 100 μM ATP (premixing concentrations). Each trace was fitted to a double exponential equation. *B*, amplitudes of the fluorescence increase upon binding of various concentrations of acto-NMIIB S1 to 0.2 μM mant-ADP. The data were fitted to a quadratic binding equation, yielding $K_5' = 0.017 \pm 0.013$ μM. *Inset*, averaged time courses of the mant-ADP fluorescence increase upon mixing 0.2 μM mant-ADP with acto-NMIIB S1 at the concentrations indicated (post-mixing concentrations are indicated). The traces were fitted to single exponentials to determine their amplitudes. *AU*, arbitrary units.

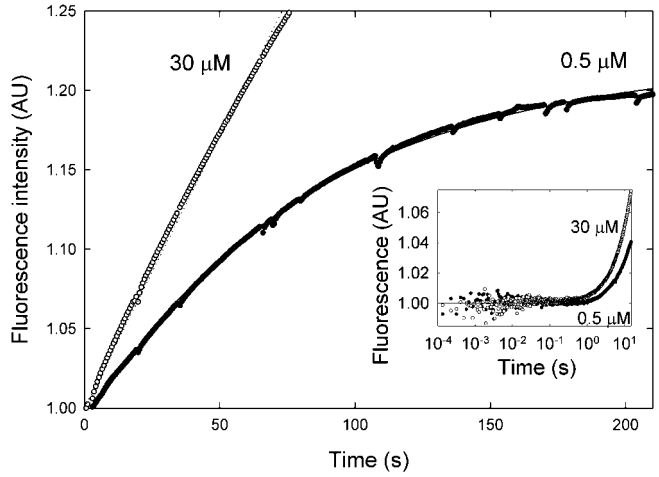

FIG. 10. **P_i release kinetics measured by stopped-flow monitoring MDCC-PBP fluorescence.** The single turnover trace shown (●) was obtained upon mixing 0.7 μM NMIIB S1 with 0.5 μM ATP, incubating for 10 s in a delay line to allow binding and hydrolysis to occur, and then mixing with 25 μM actin. The fluorescence increase was fitted to a single exponential with an observed rate constant of 0.013 s^{-1}. The time course of the reaction when 30 μM ATP was used is also shown (○). No initial burst was observed before the onset of the steady-state period. *Inset*, same reactions recorded and plotted on a logarithmic time base, where the absence of any fast phase is apparent. The amplitude of the fluorescence change in the single turnover record is in good agreement with the 5–8-fold fluorescence increase reported for MDCC-PBP upon P_i binding (16, 19). *AU*, arbitrary units.

appeared to be very weak under these conditions (an unchanged basal steady-state rate of 0.007 s^{-1} increased to only ~0.018 s^{-1} at 100 μM actin, with no observable sign of saturation), giving steady-state rates consistent with the above findings. Thus, at least under the ionic strength conditions examined, phosphate release appeared to be rate-limiting even in the presence of actin.

When double mixing experiments were carried out at 30 μM ATP, no rapid burst in P_i release was observed before the onset of the linear steady-state period of the reaction (Fig. 10), which is a further indication of phosphate release being rate-limiting in the cycle. Taking the amplitude of the single turnover transients to establish the correspondence between the extent of MDCC-PBP fluorescence change and the amount of P_i liberated, the initial slopes of the records calculated (*e.g.* 0.011 s^{-1} at 25 μM actin) were in good agreement with the observed rate constants of the single turnover reaction (0.013 s^{-1}) (Fig. 10).

DISCUSSION

The detailed kinetic properties of human NMIIB S1 were investigated in this study to unravel the functional adaptations this conventional myosin has undergone to exert its cellular function. Compared with its paralogs found in different types of muscle tissue, NMIIB S1 shows generally slower kinetics with significantly different ratios of the rate constants at certain steps of the enzymatic cycle that determine the proportions of the individual ATPase intermediates and probably also influence its mechanical properties. One striking feature of NMIIB S1 is the extent of thermodynamic coupling between the binding of actin and nucleotide. The relation of the actin and ADP binding equilibria can be deduced from the part of Scheme 1 containing the processes related to K_5', K_6, K_5, and K_{10}. In the absence of any external free energy influx or consumption, the product of the equilibrium constants viewed along one direction of the cyclic path must be 1; and thus, the ratio K_5'/K_5 should equal K_{10}/K_6. In all of the myosin II isoforms investigated, actin binding causes a reduction in the affinity for ADP and vice versa, *i.e.* the above ratios are higher than unity, although the extent of the effect varies considerably between different myosins (Table II). In the case of NMIIB S1, this ratio is between 0.2 (K_5'/K_5) and 0.4 (K_{10}/K_6). The difference between the ratios calculated from the different pairs of parameters may originate from kinetic differences that are often caused by the presence of either the mant group on the nucleotide or the pyrenyl group on actin (29) and the uncertainties caused by tight actin binding. The values obtained from ADP dissociation constants (K_5'/K_5) can be regarded as more relevant because these parameters were determined in several different types of experiment. This implies that binding of either actin or ADP has an enhancing effect on the binding of the other ligand, which is a unique feature among class II myosins.

The results obtained with the high duty ratio myosins V and VI showed a high discrepancy between the values of K_5'/K_5 and K_{10}/K_6 (18, 19), which was not detected with other myosins investigated (Table II). This difference was attributed to an

TABLE II

Acceleration of ADP release by actin and thermodynamic coupling between actin and ADP binding in different myosin isoforms

Numbering of steps refers to Scheme 1. ND, not determined.

	Acceleration k_5'/k_5	Coupling		$(K_{10}/K_6)/(K_5'/K_5)$
		K_5'/K_5	K_{10}/K_6	
NMIIB S1[a]	0.7	0.2	≈0.4	≈2
Skeletal muscle S1[b]	250	60	30	0.5
Cardiac muscle S1[c]	130	20	16	0.8
Smooth muscle S1[d]	12	4.2	6.9	1.6
Dictyostelium myosin II MHF[b]	ND	ND[e]	2.8	ND
Myosin V S1[f]	12	2.6-3.4	1500	≈500
Myosin V1 S1[g]	1.1	1.5	74	50

[a] This study.
[b] Ref. 31. MHF, myosin head fragment.
[c] Ref. 42.
[d] Ref. 23.
[e] K_5 could not be measured directly.
[f] Ref. 18.
[g] Ref. 19. T406E mutant resembling the phosphorylated form.

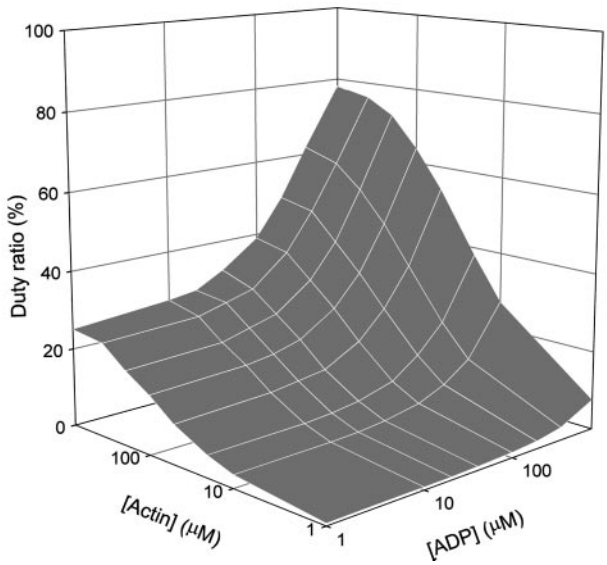

FIG. 11. **Dependence of the duty ratio on ADP and actin concentrations.** Shown are the results of kinetic simulations that were performed using a model of the acto-NMIIB S1 ATPase cycle with the experimentally determined rate and equilibrium constants. The duty ratio (*i.e.* the fraction of time spent by myosin heads in strongly actin-bound states during steady-state hydrolysis of ATP) in fact reflected the abundance of the actomyosin·ADP species because the proportion of the nucleotide-free actomyosin state was negligible throughout. The fact that the rate constant of ADP release is close to that of the rate-limiting step resulted in a considerably high duty ratio (~23%) even at very low ADP levels, which increased to ~40% in the presence of 100 μM ADP at saturating actin concentrations.

undetected isomerization of the actomyosin·ADP state similar to that proposed to occur in brush-border myosin I (30) and smooth muscle myosin (23). Nonetheless, in myosins V and VI, actin slightly reduces ADP affinity, similar to smooth muscle and *Dictyostelium* myosins (18, 19, 23, 31).

Generally, a profound effect of actin is to increase the release rate of both ADP and phosphate. ADP release is accelerated by actin by factors of 250 in skeletal, 130 in cardiac, and 12 in smooth muscle myosins (Table II) (1). The distribution of the ATPase intermediates is largely determined by the relative values of the individual rate constants. In "fast" motors such as skeletal and cardiac muscle myosins, ADP release is much faster than the steady-state ATPase rate; therefore, the actomyosin·ADP species will be present only in low abundance during steady-state ATP hydrolysis, and the duty ratio (*i.e.* the fraction of time spent in strong actin-binding states) will be low. In contrast, in high duty ratio motors such as myosins V and VI, ADP release becomes rate-limiting, resulting in high proportions of the strong actin-binding actomyosin·ADP (and actomyosin) states. We measured the rate of ADP release from acto-NMIIB S1 (k_5') to be ~0.35 s^{-1}, which is even somewhat slower than that from NMIIB S1 alone. This value is only about three times higher than the maximal steady-state actin-activated ATPase rate (0.13 s^{-1}). Thus, it appears that two steps with similar rate constants contribute to rate limitation of the overall process. In our P_i release experiments carried out at a higher ionic strength (50–100 mM) compared with the steady-state measurements, no rapid phase of P_i release was detected, unlike in experiments with skeletal muscle myosin at very low ionic strength (32) or with myosin V (18) and myosin VI (19) at 50 mM KCl. Our results show that, in NMIIB S1, P_i release is indeed rate-limiting under these conditions. If we consider the release of P_i as a two-step process consisting of the binding of myosin·ADP·P_i to actin (K_9) and the actual P_i dissociation step (K_4'; see Scheme 1) and assume that myosin·ADP·P_i and actomyosin·ADP·P_i are in rapid equilibrium ($k_9 \gg k_4'$), then the actual observed rate of P_i release will increase hyperbolically with actin concentration to plateau at k_4' (if P_i dissociation is fairly irreversible), and the actin concentration at the half-maximal rate will reflect K_9. The observed P_i release rates of NMIIB S1 did not show any sign of saturation up to 60 μM actin, which implies that the actin affinity of the myosin·ADP·P_i complex is very low ($K_9 > 50$ μM) at this ionic strength. Similar to NMIIB S1, the observed rate of P_i release from myosin V did not show saturation up to ~40 μM actin (18), whereas the K_9 values were determined to be 30–40 μM in myosin VI (50 mM KCl) (19) and 20 μM in skeletal muscle myosin (low ionic strength) (32). Thus, although no direct measurement of k_4' was possible under these conditions, we can conclude that, at physiologically relevant ionic strengths, P_i release is rate-limiting in the acto-NMIIB S1 ATPase cycle because of the high value of K_9.

We performed kinetic simulations of the enzymatic cycle with the rate constants determined experimentally. In these simulations, we set the maximal rate of P_i release (k_4') to 0.13 s^{-1} (taken from the maximal actin-activated ATPase rate) and K_9 to 59 μM assuming that it is reflected in the steady-state K_{ATPase} value. The distribution of the S1 molecules between the strongly and weakly actin-bound (or dissociated) states appeared to be determined by the relative magnitude of the phosphate and ADP release rate constants. At saturating ATP and actin concentrations, a k_4' of 0.13 s^{-1} and a k_5' of 0.35 s^{-1} resulted in ~23% of the myosin heads being in the strongly

bound actomyosin·ADP state. The actomyosin state was not significantly populated under these conditions because of the fast and tight binding of ATP. This shows that NMIIB S1 may well be an "intermediate duty ratio" motor with characteristics part way between those of skeletal or smooth muscle myosin (duty ratio of ~4%) (33) and the high duty ratio motors myosins V and VI (reported duty ratios of 70 and 80–90%, respectively) (18, 19), where the ADP release step is rate-limiting. In NMIIB S1, actomyosin·ADP·P_i remains the predominant intermediate at high actin concentrations. The time course of P_i release does not show an initial burst phase during the onset of the steady state (as it does in cases when P_i release is not rate-limiting (*cf.* Ref. 19)). Interestingly, the steady-state rate of P_i release is significantly (~30%) lower under these conditions than could be expected from the degree of saturation of the K_9 equilibrium and the maximal rate of P_i release (k_4'). This is apparently due to the ADP release rate constant (k_5') being close in value to k_4' because a marked elevation of k_5' abolishes this effect. We also investigated the effect of ADP concentration on the distribution of the steady-state ATPase intermediates. The physiological ADP concentration in the cytosol of smooth muscle cells ranges from 40 to 150 μM (34, 35). Fig. 11 shows that, in this range, the ADP concentration has a significant effect on the abundance of the actomyosin·ADP state and hence the duty ratio of the acto-NMIIB ATPase cycle, which can go up to 40% at 100 μM ADP.

The pre-steady-state kinetics presented in this study are totally consistent with those from previous steady-state ATPase and *in vitro* motility experiments (5, 11). The rate of ADP release from actomyosin·ADP is the slowest yet measured for any myosin; and because it is thought to be the kinetic step that regulates the rate of actin filament sliding, it is not surprising that NMIIB heavy meromyosin moves actin at the slow rate of ~0.05 μm/s at 25 °C (36).

NMIIB is one of three non-muscle myosin II isoforms to be part of the mammalian genome (2). By the term "non-muscle," we imply only that the expression of these myosins is not limited to one or more types of muscle cells. Indeed, non-muscle myosins have been shown to be components of skeletal muscle cells and are expressed in some smooth muscle tissues in significant amounts (37, 38). One recent study using smooth muscle myosin knockout mice even suggests an important role for non-muscle myosins in tension maintenance in smooth muscle (39). Upon prolonged activation, smooth muscle from mutant mice showed a practically unaltered slow phase force generation, with the absence of the fast peak that can be assigned to recruitment of smooth muscle myosin. Furthermore, the magnitude of phase 2 force generation corresponded to the expression level of non-muscle myosin heavy chains. Thus, a pronounced role of non-muscle myosin II in tension generation and maintenance was shown, in line with its proposed role in maintaining cortical tension in other cell types. The very low steady-state enzymatic activity of non-muscle myosins confers the obvious advantage of energetic economy within the cell.

Structural results on non-muscle myosin II filaments provide clues to how the slow ADP release and hence elevated duty ratio of NMIIB can be functionally important. These filaments have been shown to be much shorter than those of skeletal or smooth muscle myosin II. Based on electron micrographs of *in vitro* assembled non-muscle myosin II filaments, a model of the bipolar myosin minifilament consisting of ~14 myosin molecules at either end was proposed (40). Consistent with this model are the dimensions of minifilaments observed in fibroblasts (41). Considering the small number of heads in the appropriate orientation in an individual filament, the non-muscle myosin heads may need to have considerably higher time-averaged association with actin compared with muscle myosin filaments to maintain contact between individual actin filaments and to generate sufficient tension.

The differences in the localization and function of the different non-muscle myosin II isoforms are not well resolved. Whether the different isoforms can assemble into cofilaments *in vivo* is still a question. However, the hitherto unique enzymatic properties of NMIIB shed light on how the essential cellular functions in cytokinesis, cell locomotion, and tension generation and maintenance are carried out by these isoforms.

Acknowledgments—We thank Drs. Earl Homsher and Robert Adelstein for helpful comments on the manuscript, Yue Zhang for excellent technical assistance, and Dr. Howard White for the generous gift of MDCC-PBP.

REFERENCES

1. Sellers, J. R. (1999) *Myosins*, 2nd Ed., Oxford University Press, Oxford
2. Berg, J. S., Powell, B. C., and Cheney, R. E. (2001) *Mol. Biol. Cell* **12,** 780–794
3. Umemoto, S., and Sellers, J. R. (1990) *J. Biol. Chem.* **265,** 14864–14869
4. Wang, F., Harvey, E. V., Conti, M. A., Wei, D., and Sellers, J. R. (2000) *Biochemistry* **39,** 5555–5560
5. Pato, M. D., Sellers, J. R., Preston, Y. A., Harvey, E. V., and Adelstein, R. S. (1996) *J. Biol. Chem.* **271,** 2689–2695
6. Kawamoto, S., and Adelstein, R. S. (1991) *J. Cell Biol.* **112,** 915–924
7. Buxton, D. B., Golomb, E., and Adelstein, R. S. (2003) *J. Biol. Chem.* **278,** 15449–15455
8. Rochlin, M. W., Itoh, K., Adelstein, R. S., and Bridgman, P. C. (1995) *J. Cell Sci.* **108,** 3661–3670
9. Maupin, P., Phillips, C. L., Adelstein, R. S., and Pollard, T. D. (1994) *J. Cell Sci.* **107,** 3077–3090
10. Kelley, C. A., Sellers, J. R., Gard, D. L., Bui, D., Adelstein, R. S., and Baines, I. C. (1996) *J. Cell Biol.* **134,** 675–687
11. Cremo, C. R., Wang, F., Facemyer, K., and Sellers, J. R. (2001) *J. Biol. Chem.* **276,** 41465–41472
12. Takahashi, M., Kawamoto, S., and Adelstein, R. S. (1992) *J. Biol. Chem.* **267,** 17864–17871
13. Hu, A., Wang, F., and Sellers, J. R. (2002) *J. Biol. Chem.* **277,** 46512–46517
14. Spudich, J. A., and Watt, S. (1971) *J. Biol. Chem.* **246,** 4866–4871
15. Cooper, J. A., Walker, S. B., and Pollard, T. D. (1983) *J. Muscle Res. Cell Motil.* **4,** 253–262
16. Brune, M., Hunter, J. L., Corrie, J. E. T., and Webb, M. R. (1994) *Biochemistry* **33,** 8262–8271
17. Wang, F., Chen, L., Arcucci, O., Harvey, E. V., Bowers, B., Xu, Y., Hammer, J. A., III, and Sellers, J. R. (2000) *J. Biol. Chem.* **275,** 4329–4335
18. De La Cruz, E. M., Wells, A. L., Rosenfeld, S. S., Ostap, E. M., and Sweeney, H. L. (1999) *Proc. Natl. Acad. Sci. U. S. A.* **96,** 13726–13731
19. De La Cruz, E. M., Ostap, E. M., and Sweeney, H. L. (2001) *J. Biol. Chem.* **276,** 32373–32381
20. Bagshaw, C. R., Eccleston, J. F., Eckstein, F., Goody, R. S., Gutfreund, H., and Trentham, D. R. (1974) *Biochem. J.* **141,** 351–364
21. Malnasi-Csizmadia, A., Pearson, D. S., Kovacs, M., Woolley, R. J., Geeves, M. A., and Bagshaw, C. R. (2001) *Biochemistry* **40,** 12727–12737
22. Kurzawa, S. E., and Geeves, M. A. (1996) *J. Muscle Res. Cell Motil.* **17,** 669–676
23. Cremo, C. R., and Geeves, M. A. (1998) *Biochemistry* **37,** 1969–1978
24. Geeves, M. A., and Jeffries, T. E. (1988) *Biochem. J* **256,** 41–46
25. Yengo, C. M., Chrin, L. R., Rovner, A. S., and Berger, C. L. (2000) *J. Biol. Chem.* **275,** 25481–25487
26. Kovacs, M., Malnasi-Csizmadia, A., Woolley, R. J., and Bagshaw, C. R. (2002) *J. Biol. Chem.* **277,** 28459–28467
27. Ostap, E. M., and Pollard, T. D. (1996) *J. Cell Biol.* **132,** 1053–1060
28. Malnasi-Csizmadia, A., Woolley, R. J., and Bagshaw, C. R. (2000) *Biochemistry* **39,** 16135–16146
29. Taylor, E. W. (1991) *J. Biol. Chem.* **266,** 294–302
30. Jontes, J. D., Milligan, R. A., Pollard, T. D., and Ostap, E. M. (1997) *Proc. Natl. Acad. Sci. U. S. A.* **94,** 14332–14337
31. Ritchie, M. D., Geeves, M. A., Woodward, S. K. A., and Manstein, D. J. (1993) *Proc. Natl. Acad. Sci. U. S. A.* **90,** 8619–8623
32. White, H. D., Belknap, B., and Webb, M. R. (1997) *Biochemistry* **36,** 11828–11836
33. Harris, D. E., and Warshaw, D. M. (1993) *J. Biol. Chem.* **268,** 14764–14768
34. Krisanda, J. M., and Paul, R. J. (1983) *Am. J. Physiol.* **244,** C385–C390
35. Khromov, A., Somlyo, A. V., and Somlyo, A. P. (1998) *Biophys. J* **75,** 1926–1934
36. Siemankowski, R. F., Wiseman, M. O., and White, H. D. (1985) *Proc. Natl. Acad. Sci. U. S. A.* **82,** 658–662
37. Takeda, K., Yu, Z. X., Qian, S., Chin, T. K., Adelstein, R. S., and Ferrans, V. J. (2000) *Cell Motil. Cytoskeleton* **46,** 59–68
38. Rovner, A. S., Murphy, R. A., and Owens, G. K. (1986) *J. Biol. Chem.* **261,** 14740–14745
39. Morano, I., Chai, G. X., Baltas, L. G., Lamounier-Zepter, V., Lutsch, G., Kott, M., Haase, H., and Bader, M. (2000) *Nat. Cell Biol.* **2,** 371–375
40. Niederman, R., and Pollard, T. D. (1975) *J. Cell Biol.* **67,** 72–92
41. Verkhovsky, A. B., Svitkina, T. M., and Borisy, G. G. (1995) *J. Cell Biol.* **131,** 989–1002
42. Siemankowski, R. F., and White, H. D. (1984) *J. Biol. Chem.* **259,** 5045–5053

Kinetic Mechanism of Non-muscle Myosin IIB: FUNCTIONAL ADAPTATIONS FOR TENSION GENERATION AND MAINTENANCE

Fei Wang, Mihály Kovács, Aihua Hu, John Limouze, Estelle V. Harvey and James R. Sellers

J. Biol. Chem. 2003, 278:27439-27448.
doi: 10.1074/jbc.M302510200 originally published online April 17, 2003
